Large differences in the electronic structure and spectroscopic properties of three phases of $AlPO_4$ from *ab initio* calculations

W. Y. Ching and Paul Rulis
Department of Physics, University of Missouri-Kansas City, Kansas City, Missouri, 64110 USA
(Received 14 February 2008; published 12 March 2008)

The electronic structure, interatomic bonding, and spectroscopic properties of the three known phases of $AlPO_4$ in trigonal, orthogonal, and monoclinic structures formed at different pressures were studied using the density functional method. These three crystals have the same chemical formula and the same percentages of different atomic species but distinct local atomic coordination which offers a unique opportunity to systematically investigate their structure-properties relationship. The Al-*K*, Al-L_3, P-*K*, P-L_3, and O-*K* x-ray absorption near edge structure (XANES) edges were calculated using a supercell approach including the effects of core hole. The large differences in these properties among the three crystals are demonstrated and explained in terms of the unique structural units present in each phase. These results are in contradiction to the prevailing notion of using fingerprinting for XANES spectra interpretation.

DOI: 10.1103/PhysRevB.77.125116 PACS number(s): 78.70.Dm, 71.20.−b, 78.66.Nk

I. INTRODUCTION

Phosphates are a large class of compounds containing radical phosphorus and oxygen with a formal charge of −3 denoted by PO_4^{-3}. PO_4 also occurs in many biomolecular systems such as DNA or cobalamins (vitamin B_{12}). Among the inorganic crystals, $AlPO_4$ is a subclass of network oxides with a structure in close analogy to α quartz. Over the years, α-$AlPO_4$ (berlinite) has been extensively studied both experimentally[1–6] and theoretically,[7–10] focusing mostly on the structural transformation under pressure and the related phenomenon of reversible amorphization.[1,4] It was reported and confirmed by molecular dynamic simulations that at a pressure of around 13 GPa, berlinite transforms into a new orthorhombic phase of space group *cmcm* (denoted hereafter as *o*-$AlPO_4$) in which Al is octahedrally coordinated.[5] Very recently, it was reported that at a still higher pressure of 97.5 GPa, $AlPO_4$ further transforms into a monoclinic structure (denoted as *m*-$AlPO_4$).[11] In this structure, the P ion becomes octahedrally bonded instead of tetrahedrally bonded as in the α and *o* phases. Here, a sixfold coordinated PO_6 bonding unit has been observed and it has tremendous implications on the structural chemistry of phosphates at high pressure.

In contrast to the extensive investigations of the structural properties of $AlPO_4$ under pressure, the electronic structure and bonding of the $AlPO_4$ phases, with the exception of berlinite,[8,9] have not been well studied. The systematic variation of the coordination changes and the availability of high precision structural data for the three phases (α-, *o*-, and *m*-$AlPO_4$) offers a unique opportunity to delineate the Al-O and P-O bonding in the $AlPO_4$ system. In particular, the x-ray absorption near edge structure (XANES) is very sensitive to the local bonding environment of the ions in the crystal and has been used as an effective characterization tool for many inorganic compounds. A prevailing concept in interpreting the measured XANES spectra is the so-called fingerprinting which essentially says that the XANES edge of an ion can be predicted based on specific local nearest neighbor bonding configuration or vice versa. The three phases of $AlPO_4$ provide an ideal case to test the validity of such a claim because of their clear-cut local structure. In α-$AlPO_4$, both Al and P are fourfold coordinated and both O sites (O1 and O2 in equal proportions) are bridging between Al and P. In *o*-$AlPO_4$, Al becomes sixfold coordinated and P remains fourfold coordinated. O1 is now in a threefold bond to two Al and one P, whereas O2 remains in the bridging configuration. In *m*-$AlPO_4$, both Al and P are sixfold coordinated and both O are threefold coordinated. O1 bonds to one Al and two P and O2 bonds to two Al and one P. These variations in local bonding for crystals with the same formula unit and same types of atoms in equal proportions offer a very rare opportunity for precise characterization of their XANES spectra in relation to their structural variations. In this paper, we report the results of *ab initio* calculations of the electronic structure, bonding, and optical properties of the three phases of $AlPO_4$. We have also calculated all relevant XANES edges (Al-*K*, Al-L_3, P-*K*, P-L_3, and O-*K*) in these crystals. We found large differences among them that are in contradiction to the notion of fingerprinting. Our calculations are timely investigations for the *o*-$AlPO_4$ and *m*-$AlPO_4$ phases.

The layout of this paper is as follows. We briefly discuss the methods of our calculations in the next section. This is followed by the presentation of the results and a discussion of them in Sec. III. We briefly summarize our findings in Sec. IV.

II. METHOD OF CALCULATIONS

We used the experimentally determined structure for α-$AlPO_4$ (Ref. 12) and the other two high pressure phases.[11] The crystal structure information is listed in Table I. The first-principles orthogonalized linear combination of atomic orbitals (OLCAOs) method was used.[13] The OLCAO method is a density-functional theory (DFT) based method using the local density approximation (LDA) to the exchange-correlation potential and has been demonstrated to be very effective for crystals of complex structures and large unit cells. In the present calculation, the basis function consists of

TABLE I. Structure and electronic properties of three phases of $AlPO_4$. The number in parentheses for BL is the number of such bonds.

Crystal	α-$AlPO_4$	o-$AlPO_4$	m-$AlPO_4$
Space group	$P3_221$ (154)	$Cmcm$ (63)	$P2/m$ (10)
Cell parameters a, b, c, (Å)	4.958, 4.958, 10.967	5.0365, 7.2908, 5.7491	3.838, 2.506, 4.036
			β=87.4°
Z	3	2	1
E_g (eV)	5.71	6.32	4.01
$\varepsilon_2(0)$	2.495	3.246	5.074
Q^* (electrons)			
Al	1.173	1.387	1.268
P	2.720	2.701	3.305
O1	7.020	6.964	6.839
O2	7.030	6.991	6.875
Al-O BO	0.217, 0.224	0.163, 0.191	0.158, 0.308
[BL (Å)]	(1.727) (2)	(1.913) (4)	(1.745) (2)
	(1.738) (2)	(1.818) (2)	(1.716) (4)
Total BO	0.441	1.034	1.532
P-O BO	0.316, 0.308	0.263, 0.365	0.285, 0.194
	(1.524) (2)	(1.576) (2)	(1.879) (4)
	(1.518) (2)	(1.463) (2)	(1.503) (2)
Total BO	0.624	1.256	1.346
Supercell (No. of atoms)	$2\times2\times1$ (72)	$2\times2\times2$ (96)	$2\times3\times2$ (72)

atomiclike orbitals of $1s,2s,3s,4s,2p,3p,4p,3d$ for Al and P and $1s,2s,3s,2p,3p$ for O. Additional orbitals were added for the optical and XANES spectral calculations to increase the accuracy of the higher unoccupied states. A large number of k points were employed for integration over the irreducible portion of the Brillouin zone (BZ) which is necessary for accurate calculation of the spectral properties and the evaluation of the density of state (DOS). Supercells were used for the XANES calculation for the three crystals which were tested to be sufficiently large (see Table I) to ensure that spurious interactions between the core holes in adjacent cells are negligible.[14] The exact procedures of the calculation have been described in many recent papers.[14–20] We briefly recapture the essential points here. The initial state of each edge is the ground state of the target atom in the supercell. The final states, calculated separately, are the conduction band states with the excited electron from the targeted core placed at the bottom of the conduction band (CB). It should be pointed out that in the final state calculation, the system remains charge neutral by including the electron in the otherwise empty CB in the charge density accumulation for the self-consistent potential. The interaction between the excited electron in the CB and the hole that was left behind is fully accounted for in the self-consistent iterations of the final state calculation. This core-hole effect can significantly modify the final state wave function and hence the XANES spectrum. The final XANES edges are obtained by evaluating the transition strength in the dipole approximation and include the dipole matrix elements between the initial state ($1s$ for the K-edge and $2p$ for the L edge) and the final states (core-hole states). The inclusion of the dipole matrix elements calculated from the ab initio wave functions automatically ensures that the selections rules are fully satisfied. All calculated final spectra are broadened by a Gaussian with a full width at half maximum of 1.0 eV for consistency. For easy comparison, all spectra for the same edge are normalized to the same area.

III. RESULTS AND DISCUSSION

A. Electronic structure and bonding

The calculated band structures of the three crystals are shown in Fig. 1. The band structure of berlinite is almost identical to that in Ref. 8. The calculated LDA band gaps (E_g) are 5.71, 6.32, and 4.01 eV for α-, o-, and m-$AlPO_4$, respectively. E_g for o-$AlPO_4$ and m-$AlPO_4$ are direct at Γ and that for α-$AlPO_4$ is indirect with the top of the Valence band (VB) at the K point. The bottoms of the CB are all at Γ for the three crystals. The real band gap will be somewhat larger since LDA-DFT calculations generally underestimate

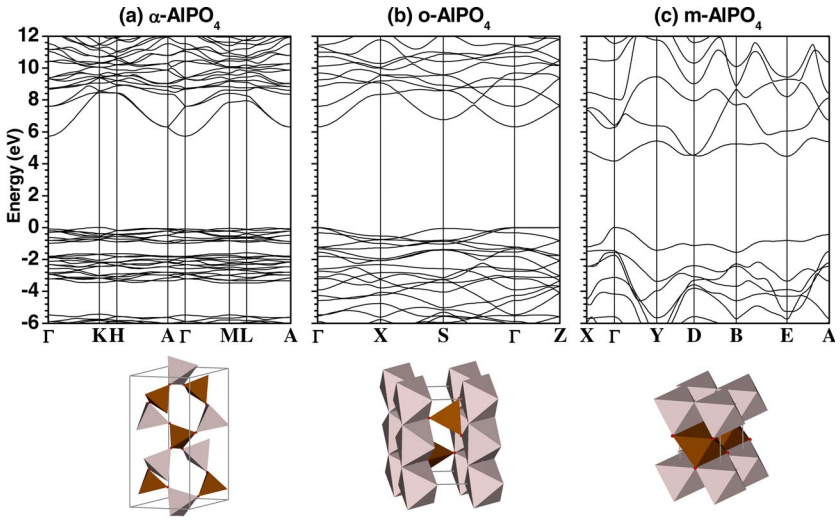

FIG. 1. (Color online) Band structures of (a) α, (b) o, and (c) m phases of $AlPO_4$. Also shown are the ball and stick sketches of the crystals showing the octahedral or tetrahedral units of the cations.

the real band gaps. It is interesting to note that the largest E_g is with o-$AlPO_4$. The bands in the three crystals show great variations in band curvatures at both the VB and CB edges. The calculated DOS and atom-resolved partial DOS (PDOS) are shown in Fig. 2. From the partial PDOS, interactions between orbitals of different ions can be easily identified. The upper VB involves bonding with O $2p$ orbitals. In berlinite, it has four segments, whereas in the other two crystals, they merged into a single band with a significantly increased band width in the case of $m$$AlPO_4$. The interaction between O $2p$ and cation orbitals in this energy range involves s, p, and d orbitals of both Al and P with contributions from Al $3d$ and P $3d$ orbitals at the upper VB. The two peaks at the lower energy involve the interaction between the O $2s$ orbitals with the cations. The splitting into two peaks (or segments) originates from interaction with either Al or P as in the case of α-$AlPO_4$. In o-$AlPO_4$ and m-$AlPO_4$, O1 and O2 are progressively found to bond to Al and P involving all cation orbitals, resulting in the more complex and wider structures. In the CB region, there are also drastic differences

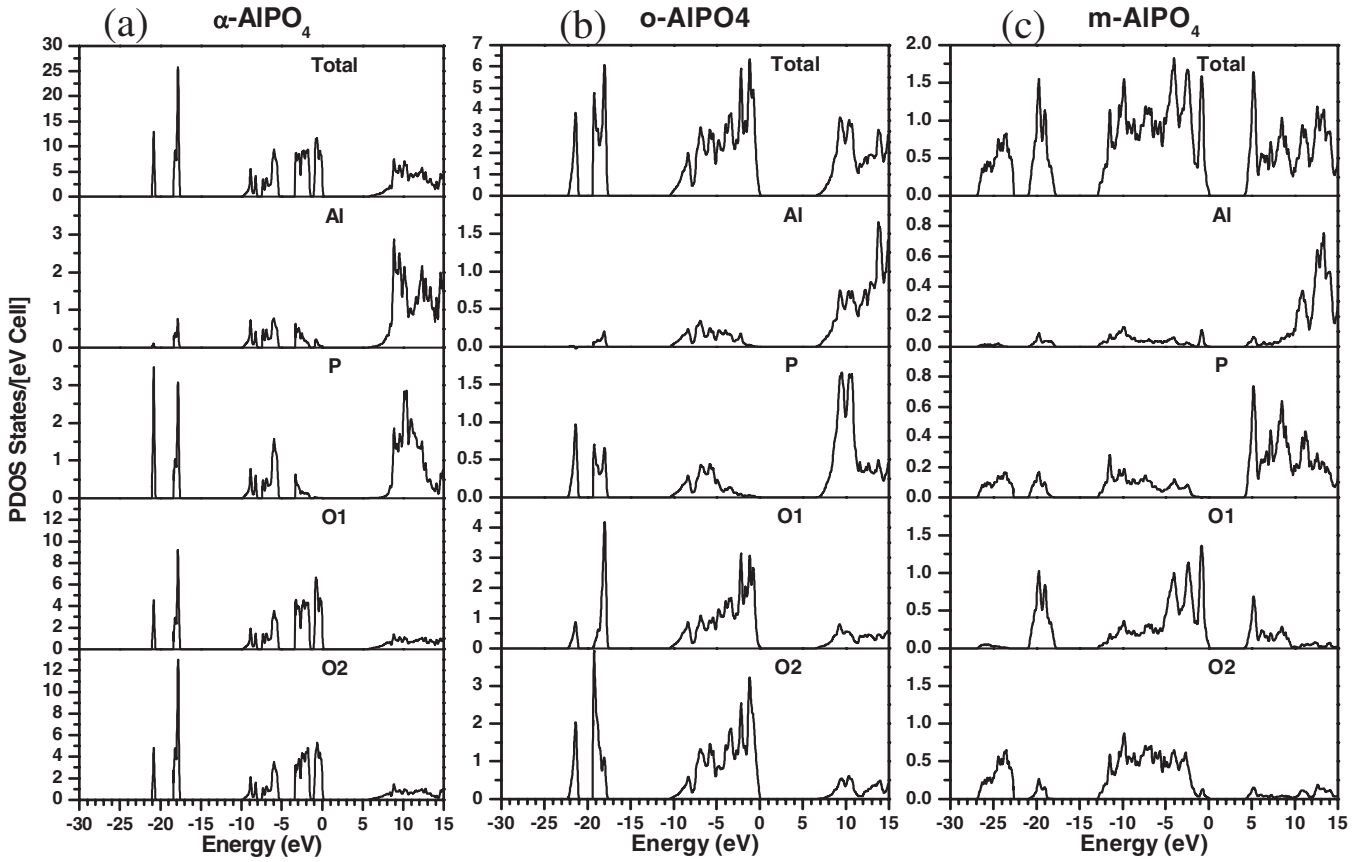

FIG. 2. Calculated total and partial DOS of (a) α-$AlPO_4$, (b) o-$AlPO_4$, and (c) m-$AlPO_4$.

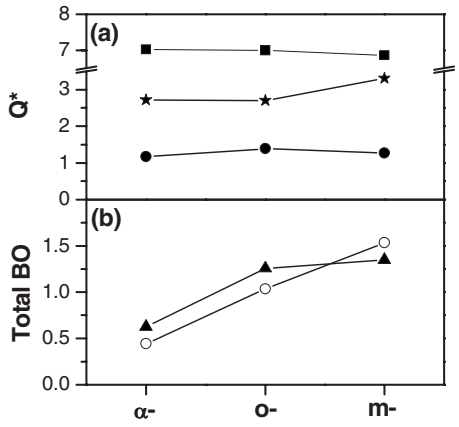

FIG. 3. (a) The calculated effective charges Q^*: circle (Al), star (P), and square (O). (b) Total BO for the Al (open circle) and P (solid triangle) tetrahedral and octahedral units in three crystals.

in the DOS. In α-$AlPO_4$ and o-$AlPO_4$, the lower CB states are from the Al ions, while those from P are at a higher energy. In o-$AlPO_4$, the relative separations of the CB states originating from Al and P are reduced and in m-AlO_4 the P states are shifted below the Al states with the sharp peak at the CB edge purely from P s states.

The above results on the electronic structure show that the changes from α-$AlPO_4$ to o-$AlPO_4$ to m-$AlPO_4$ do not simply scale with density by shifting the peak structure or varying the band width. Definitely, a delicate interplay of crystal symmetry and the presence of different types of cation polyhedra dictate the overall electronic structure. All these indicate that the drastic changes in the structural units from (AlO_4, PO_4) to (AlO_6, PO_4) and eventually to (AlO_6, PO_6) in going from α- to o- to m-$AlPO_4$ have significant influence of the electron states and bonding in both the VB and CB regions. In order to be more quantitative, we also describe the electronic structure and bonding in the three crystals in terms of the Mullikan effective charges Q_α^* and the interatomic bond orders (BOs) $\rho_{\alpha\beta}$ between pairs of atoms.[21] They are listed in Table I and Fig. 3 together with the bond lengths (BLs) and the number of the bonds for a particular BL. Q^* for the Al (P) changed from 1.173 (2.720) to 1.387 (2.701) to 1.268 (3.305) in going from α- to o- to m-$AlPO_4$ phases, indicating a gradual increase in the covalent character of the bonds since there are less charge transfers from cation to O in the series. The average Q^* for O decreases from 7.025 to 6.978 and then to 6.857 in the same sequence. It is noted that Q^* of the cations have large increases from the fourfold to the sixfold coordination. The BO values, which depend on BLs, quantify the strength of particular bonds at the equilibrium separations. Since the basic structural units in these three crystals are corner-sharing or edge-sharing tetrahedra and octahedra with different BLs, it is much more meaningful to compare the total BO within the respective structural units by summing over individual bonds. Figure 3 shows a very interesting fact that the total BO for P-O_4 is greater than that of Al-O_4 and Al-O_6 in α-$AlPO_4$ and o-$AlPO_4$, but the total BO for Al-O_6 is greater than that of P-O_6 in m-$AlPO_4$. Previously, no one has ever encountered the octahedral bonding with P, and this should have significant implications in understanding the interatomic bonding in phosphates.

B. Optical properties

The calculated complex dielectric functions of the three crystals using the *ab initio* wave functions and a large number of k points in the BZ integration are displayed in Fig. 4. They again show substantial differences. For the imaginary part $\varepsilon_2(\hbar\omega)$ [Fig. 4(b)], both α-$AlPO_4$ and o-$AlPO_4$ have a footlike structure at the absorption onset [Fig. 4(c)], indicating that the direct transition at Γ is symmetry forbidden. However, there is no such footlike structure for m-$AlPO_4$; instead, there is a prominent first peak at about 6.7 eV. The footlike structure at the absorption onset implies that any measured optical gap in these crystals will be larger than the calculated LDA gap, or the intrinsic gap. This is in addition to the general observation that DFT calculations always underestimate the band gap of insulators. There is also a steady increase in absorptions above 25 eV from α- to o- to m-$AlPO_4$ that are related to the increased mass density in the series.

The real part of the dielectric function $\varepsilon_1(\hbar\omega)$ [Fig. 4(a)] is obtained from $\varepsilon_2(\hbar\omega)$ by Kramers–Kronig conversion. The calculated optical static dielectric constants, $\varepsilon_1(0)$, for the three crystals are 2.50, 3.25, and 5.07, respectively. This trend does not follow the size of the band gap as generally assumed for insulators. The square root of $\varepsilon_1(0)$ can be related to the average refractive index n of the material. The reported value of n for α-$AlPO_4$ is 1.54 (Ref. 22) which is quite close to the calculated value of $\sqrt{\varepsilon_1(0)}=1.580$. The $\varepsilon_2(\hbar\omega)$ spectrum for α-$AlPO_4$ is in good agreement with the vacuum ultraviolet optical measurement of Tan and French.[23] The six prominent features above the excitonic peak are all reproduced as marked by the arrows in Fig. 4(b).

C. X-ray absorption near edge structure spectra

We now discuss the large differences of the XANES spectra in the three crystals. XANES spectra have been used as one of the most effective characterization tools for many other phosphates of practical importance, for example, in phosphates used for molecular sieves.[24,25] Proper interpretation of the measured spectra requires a fundamental knowledge of the edge spectra in phosphates with well defined local geometric configurations. The 18 spectra for the three crystals are displayed in Fig. 5. They are Al-K, Al-L_3, P-K, P-L_3, and O-K (O1 and O2) edges. The spectacular differences of these spectra are in the different types of bonding in the three crystals. We focus our discussion on three aspects: (1) the shape and the number of prominent peaks, (2) the location and the relative positions of these peaks, and (3) the energy and the structure of the edge onset. They are discussed in the context of the local coordination for each ion and to ascertain the validity of the fingerprinting technique for edges prediction. The only experimental data we can find is the P-K edge in α-$AlPO_4$,[26] which is in close agreement with the calculation.

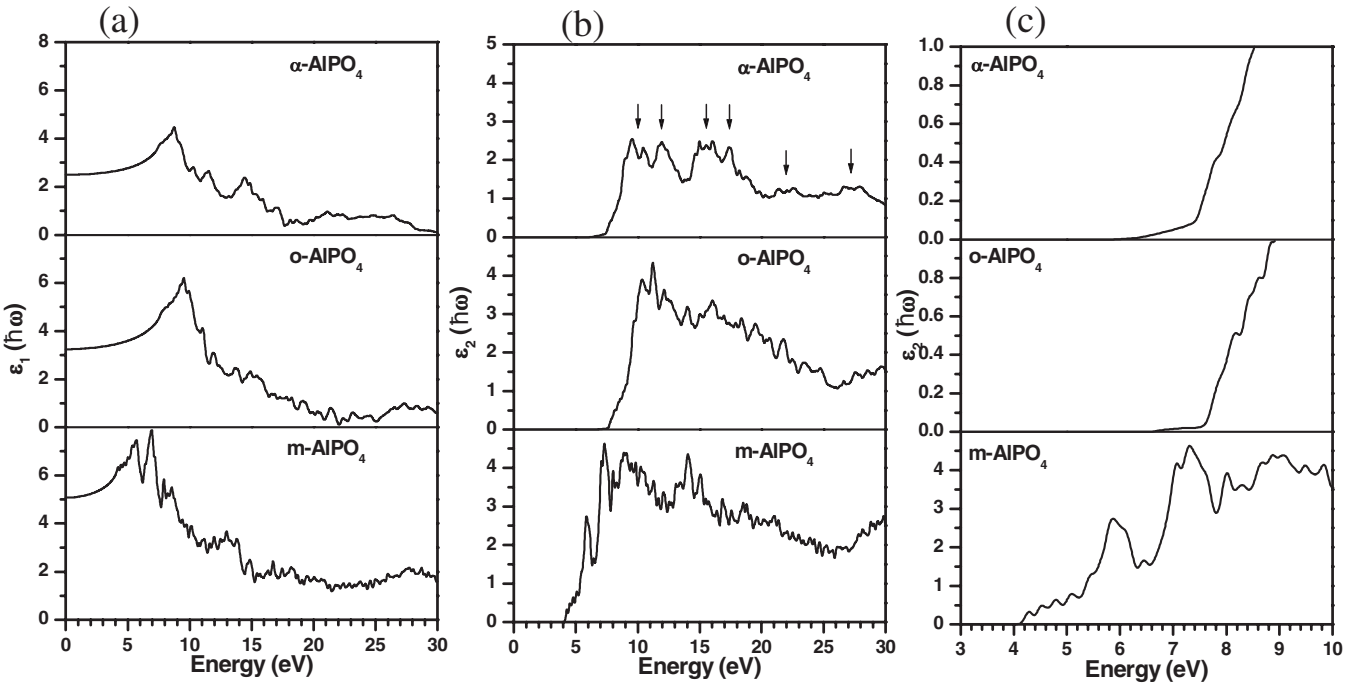

FIG. 4. Calculated (a) real and (b) imaginary parts of the complex dielectric functions for α-$AlPO_4$, o-$AlPO_4$, and m-$AlPO_4$. (c) The absorption near the onset in three crystals, showing the footlike structure for α-$AlPO_4$, o-$AlPO_4$.

Figure 5(a) shows the Al-K edges in three crystals with Al-O_4 and Al-O_6 coordinations [Figs. 5(a1), 5(a2), and 5(a3)]. The differences between them are very obvious in the locations and amplitudes of the peaks. The sixfold Al-K spectra have lower absorption edges. The conspicuous part is the difference between Figs. 5(a2) and 5(a3), both Al-K have octahedral environments, yet the spectra are very different. In particular, the Al-K edge in m-$AlPO_4$ [Fig. 5(a3)] does not have a sharp edge onset. This is because the lowest CB in m-$AlPO_4$ consists of P orbitals and have little admixture from Al components. It has three well defined peaks within the first 15 eV from the edge onset while o-$AlPO_4$ [Fig. 5(a2)] has five structures within the same energy range. The same quantitative difference can be seen in the Al-L_3 edges of Fig. 5(b). In this case, tetrahedral Al [Fig. 5(b1)] shows a lot more structures than the octahedral Al [Figs. 5(b2) and 5(b3)]. As in the case of Al-K, the two spectra for the sixfold coordinated Al in o-$AlPO_4$ and m-$AlPO_4$ are very different. Figure 5(b2) shows three prominent peaks, whereas Fig. 5(b3) shows only two. The edge onset of the later is again not abrupt. The main peaks near 100 eV have different symmetric shapes in the two crystals. The centroid of the peak in o-$AlPO_4$ is at the lower energy.

The P-K edges for the tetrahedral P and octahedral P show big differences and a steady shift to lower absorption energy in going from α- to o- to m-$AlPO_4$. The sixfold P [Fig. 5(c3)] has a well-resolved double peak near the edge onset and more complex spectral features above the double peak. In contrast, the fourfold P [Figs. 5(c1) and 5(c2)] has a very sharp leading peak at the absorption onset and two smaller peaks in the next 10 eV range. The two P-K edges with fourfold coordination in α-$AlPO_4$ and o-$AlPO_4$ are quite similar although there are still differences in the intensities near the minimum above the main peak and the higher peak 11 eV above it. This is the closest case that a spectrum may be predicted by the fingerprinting argument based on the local structure. The only experimental data[26] available is for P-K in α-$AlPO_4$ which shows excellent agreement with the calculation [Fig. 5(c1)]. The dramatic difference in the K edges of the fourfold and sixfold coordinated P can also be seen in the P-L_3 spectra in Fig. 3(d). In this case, the fourfold P has three well defined peaks, whereas the sixfold P has much more complex spectral features. In contrast to the similarities between Figs. 5(c1) and 5(c2) for the K edge, there is a noticeable difference between Figs. 5(d1) and 5(d2) for the L_3 edges. The middle peak around 148 eV in o-$AlPO_4$ is much less sharp than the same peak at 150 eV in α-$AlPO_4$.

We now turn to O-K edges for both O1 and O2 in the three crystals shown in Figs. 5(e) and 5(f), respectively. These six O-K edges can be divided into three cases: (1) bridging O between an Al and a P [Figs. 5(e1), 5(f1), and 5(f2)], (2) threefold bonded O to two Al and one P [Figs. 5(e2) and 5(f3)], and threefold bonded O to one Al and two P [Fig. 5(e3)]. The differences and similarities between the groups are intriguing. The threefold O's bonding to two P [Fig. 5(e3)] or two Al [Fig. 5(f3)] have more structures and sharp edge onsets and are distinctively different from other O-K edges. Even within the same group of threefold bonding to two Al [Fig. 5(e2) and 5(f3)], there are huge differences in the shape and the number of peaks. These could be partially explained by the different cation-O BLs. The two P-O BLs of 1.879 Å for O1 in m-$AlPO_4$ [Fig. 5(e3)] are much longer than the normal O-P BL. The two Al-O BLs of 1.913 Å for

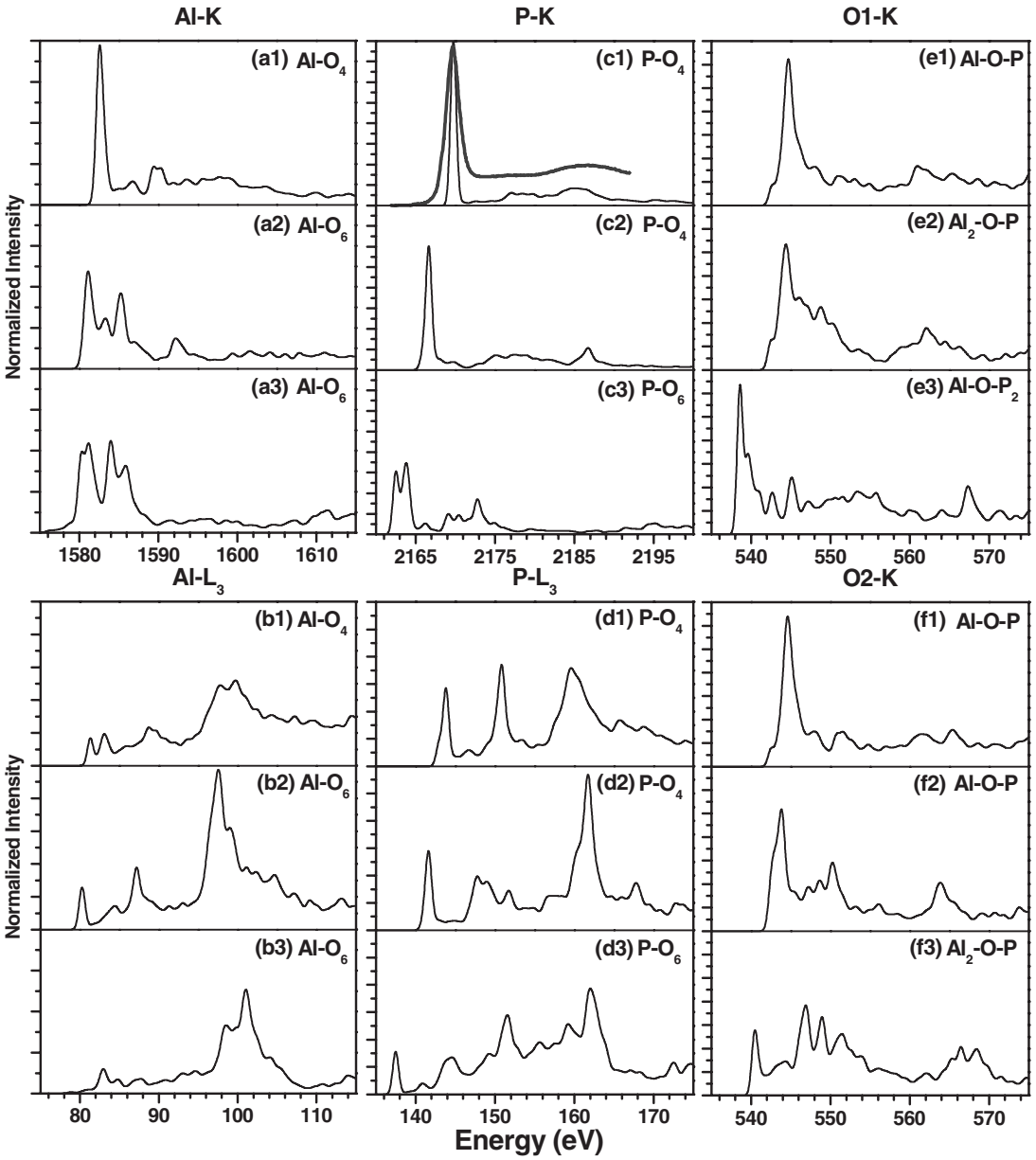

FIG. 5. Calculated XANES spectra in three crystals: (a) Al-K, (b) Al-L_3, (c) P-K, (d) P-L_3, (e) O1-K, and (f) O2-K edges. In each panel, the subpanels from 1 to 3 stand for α-$AlPO_4$, o-$AlPO_4$, and m-$AlPO_4$, respectively. The heavy line in (c1) for P-K is the experimental data from Ref. 26 with the main peak aligned.

O1 in o-$AlPO_4$ [Fig. 5(e2)] are also much longer than other Al-O separations. On the other hand, the single O-P BL of 1.463 Å for O2 in o-$AlPO_4$ is shorter than usual. The sensitive dependence of the edge spectra on the BLs renders simple fingerprinting techniques intractable. Another strong point of evidence for the failure of the fingerprinting notion is the apparent similarity in spectral shape between Figs. 5(e1) and 5(e2) which have different local bonding configurations. On the other hand, O with the same bonding configurations [Figs. 5(e2) and 5(f3)] have completely different spectra. If the measurements of the O-K edges in these crystals are conducted, it is unlikely that such detailed differences can be resolved because the measured spectra will be the average of the O1 and O2 sites. This underscores the importance of using theoretically calculated spectra to trace the source of the difference of the spectra from different sites.[20]

IV. SUMMARY

In conclusion, we have used a state-of-the-art computational method to study the electronic structures, bonding, and spectroscopic properties in three $AlPO_4$ phases formed at different pressures. The large differences found in relation to their unique but well defined structural units provide insights in understanding their property-structural relationship. From the careful comparisons of all the calculated XANES spectra

in the three crystals (Al-*K*, Al-*L*, P-*K*, P-*L*, and O-*K*) with distinctively different local atomic coordination, we conclude that the longstanding conviction of using fingerprinting for XANES spectra interpretation has not been validated. It is still likely that a simple finger printing technique may be valid, but only in the simplest cases such as in diamond and graphite.

ACKNOWLEDGMENTS

This research is supported by the U.S. Department of Energy under the Grant No. DE-FG02-84DR45170. This research used the resources of NERSC supported by the Office of Science of DOE under Contract No. DE-AC03-76SF00098.

[1] M. B. Kruger and R. Jeanloz, Science **249**, 647 (1990).
[2] A. Jayaraman, D. L. Wood, and R. G. Maines, Sr., Phys. Rev. B **35**, 8316 (1987).
[3] A. Polian, M. Grimsditch, and E. Philippot, Phys. Rev. Lett. **71**, 3143 (1993).
[4] P. Gillet, J. Badro, B. Varrel, and P. F. McMillan, Phys. Rev. B **51**, 11262 (1995).
[5] S. M. Sharma, N. Garg, and S. K. Sikka, Phys. Rev. B **62**, 8824 (2000).
[6] I. Gregora, N. Magneron, P. Simon, Y. Luspin, N. Raimoux, and E. Philippot, J. Phys.: Condens. Matter **15**, 4478 (2003).
[7] J. S. Tse and D. D. Klug, Science **255**, 1559 (1992).
[8] D. M. Christie, N. Troullier, and J. M. Chelikowsky, Solid State Commun. **98**, 923 (1996).
[9] K. C. Mishra, I. Osterloh, H. Anton, B. Hannebauer, P. C. Schmidt, and K. H. Johnson, J. Mater. Res. **12**, 2183 (1997).
[10] L. M. Ramaniah, S. M. Sharma, K. Kunc, N. Garg, and M. Laghate, Phys. Rev. B **68**, 014119 (2003).
[11] J. Pellicer-Porres, A. M. Saitta, A. Polian, J. P. Itie, and M. Hanfland, Nat. Mater. **6**, 698 (2007).
[12] Y. Muraoka and K. Kihara, Phys. Chem. Miner. **24**, 243 (1997).
[13] W. Y. Ching, J. Am. Ceram. Soc. **73**, 3135 (1990).
[14] Shang-Di Mo and W. Y. Ching, Phys. Rev. B **62**, 7901 (2000).
[15] Shang-Di Mo and W. Y. Ching, Appl. Phys. Lett. **78**, 3809 (2001).
[16] W. Y. Ching, Shang-Di Mo, and Yu Chen, J. Am. Ceram. Soc. **85**, 11 (2002).
[17] W. Y. Ching, L. Ouyang, P. Rulis, and I. Tanaka, Phys. Status Solidi B **242**, R94 (2005).
[18] W. Y. Ching and Paul Rulis, Phys. Rev. B **73**, 045202 (2006).
[19] S. Aryal, P. Rulis, and W. Y. Ching, Am. Mineral. **93**, 114 (2008).
[20] W. Y. Ching and P. Rulis, Phys. Rev. B **77**, 035125 (2008).
[21] The effective charge and the bond order (BO) are calculated according to $Q^*_\alpha = \Sigma_i \Sigma_{n,occ} \Sigma_{j,\beta} C^{*n}_{i\alpha} C^n_{j\beta} S_{i\alpha,j\beta}$ and $\rho_{\alpha\beta} = \Sigma_{n,occ} \Sigma_{i,j} C^{*n}_{j\beta} C^n_{j\beta} S_{i\alpha,j\beta}$, where $C^n_{j\beta}$ are the eigenvector coefficients and $S_{i\alpha,j\beta}$ are the overlap integrals between the ith orbital of the αth atom and jth orbital of the βth atom. The maximum BO for a pair of perfect covalently bonded atoms is 0.5 (1.0 if both spins are counted).
[22] W. L. Bond, J. Appl. Phys. **36**, 1674 (1965).
[23] G. L. Tan and R. H. French, Mater. Sci. Eng., A **422**, 136 (2006).
[24] I. D. Burton, J. S. J. Hargreaves, D. J. Nicholson, M. H. Nilsen, and M. Stockenhuber, J. Mater. Chem. **11**, 1441 (2001).
[25] A. M. Beale, A. M. J. van der Eerden, D. Grandjean, A. V. Petukhov, A. D. Smith, and B. M. Weckhuysen, Chem. Commun. (Cambridge) **2006**, 4410.
[26] R. Frank and J. Hormes, Physica B **216**, 85 (1995).